$ZnFe_2O_4$ Nanocrystals: Synthesis and Magnetic Properties

Changwa Yao,[†] Qiaoshi Zeng,[†] G. F. Goya,[‡] T. Torres,[‡] Jinfang Liu,[†,§] Haiping Wu,[†] Mingyuan Ge,[†] Yuewu Zeng,[†,||] Youwen Wang,[†,||] and J. Z. Jiang*[,†]

International Center for New-Structured Materials (ICNSM) and Laboratory of New-Structured Materials, Department of Materials Science and Engineering, and Analysis and Testing Centre, Zhejiang University, Hangzhou 310027, People's Republic of China, and Instituto Universitario de Investigación en Nanociencia de Aragón (INA), Cerbuna 12, 50009 Zaragoza, Spain

Received: April 29, 2007; In Final Form: June 18, 2007

Ferromagnetic zinc ferrite nanocrystals at ambient temperature were synthesized via the thermal decomposition of metal−surfactant complexes. Characterization measurements including transmission electron microscopy and X-ray diffraction were performed for as-synthesized $ZnFe_2O_4$ particles. The sample has a relatively narrow size distribution with an average particle size of 9.8 ± 0.2 nm and standard deviation of 30%. The as-synthesized zinc ferrite nanocrystals are superparamagnetic at room temperature with a blocking temperature $T_B = 68 \pm 2$ K and a saturation magnetization $M_S = 65.4$ emu·g^{-1} at $T = 10$ K, which are caused by the change in the inversion degree of the spinel structure. A coercive field of $H_C = 102 \pm 5$ Oe in the blocked state indicates small particle anisotropy, although evidence of surface spin canting was inferred from magnetization data in the as-synthesized $ZnFe_2O_4$ nanocrystals. Our results demonstrate that magnetic properties of magnetic particles can be largely modified by just changing particle size, which might be a useful way to design novel magnetic materials.

1. Introduction

The manufacture of magnetic nanoparticles (MNPs) started many years ago, and currently there are reliable synthesis routes. However, synthesizing MNPs of a few nanometers, keeping the magnetic moment of the corresponding bulk material, is still a challenge because the high surface/volume ratio makes the surface disorder effect to be dominant.[1] Therefore, the development of synthesis methods, by which materials, having nanometer-sized grain size, retain the magnetic performance of the bulk materials, is still desirable.

When the size of magnetic particles decreases into nanometer-sized scale, the surface area increases greatly, resulting in novel phenomena. Superparamagnetism, magnetic quantum tunneling and spin-glass-like behavior are some examples in the field of nanomagnetism.[2] These magnetic properties make magnetic nanoparticles to have many technological applications including magnetic data storage, ferrofluid, medical imaging, drug targeting, and catalysis.[3−5] The zinc ferrite, $ZnFe_2O_4$, one of the iron-based cubic spinel series, shows striking changes in its magnetic properties by reducing the grain size to the nanometer-sized range. Bulk zinc ferrite is a completely normal spinel structure with Zn ions in the tetrahedral or A sites and Fe ions in the octahedral or B sites. Due to antiferromagnetic (AFM) super-exchange interactions between B−B ions, bulk zinc ferrite is antiferromagnetic at $T_N = 10$ K. However, the magnetic structure of $ZnFe_2O_4$ can be largely altered by developing a non-equilibrium state, i.e., redistribution of iron ions at A and B sites, as $(Zn_{1-x}Fe_x)[Zn_xFe_{2-x}]O_4$, where parentheses and square brackets denote the A and B sites, respectively and the x is the inversion parameter.[6] Net magnetization at ambient temperature can be obtained in nanometer-sized $(Zn_{1-x}Fe_x)[Zn_xFe_{2-x}]O_4$ particles.[6] Various synthesis methods, such as dry- and wet-milling,[6−9] sol−gel,[10,11] co-precipitation,[12,13] microemulsions,[14] pulsed laser deposition,[15] electrodeposition,[16] thermal solid-state reaction,[17,18] and ultrasonic cavitation approach,[19] have been reported to prepare nanometer-sized $(Zn_{1-x}Fe_x)[Zn_xFe_{2-x}]O_4$ particles. Here we report a simple method to prepare $(Zn_{1-x}Fe_x)[Zn_xFe_{2-x}]O_4$ nanocrystals with a relatively narrow size distribution by thermal decomposition of organometallic precursors in high boiling point solvent octyl ether, which has been used to synthesize different monodisperse nanocrystals.[20−24] We discuss the structure and magnetic data of as-synthesized $(Zn_{1-x}Fe_x)[Zn_xFe_{2-x}]O_4$ nanoparticles.

2. Experimental Details

2.1. Chemicals. All the chemical reagents in our experiments were used without any purification. The precursor $ZnAc_2 \cdot 2H_2O$ (99.99%) and oleic acid (90%) were purchased from Alfa Aesar company, and the other precursor $Fe(CO)_5$ was purchased from Sigma-Aldrich. High boiling point solvent octyl ether (99%) was purchased from Tokyo Kasei Kogyo Co. Anhydrous ethanol (C_2H_5OH, chromatogram grade) was purchased from Scharlau Chemie S.A.

2.2. Synthesis of Nanometer-Sized Zinc Ferrite $ZnFe_2O_4$. In a typical experiment, 0.11 g (0.5 mmol) of $ZnAc_2 \cdot 2H_2O$ and 5 mL of anhydrous ethanol were placed in a 50 mL beaker. The mixture was heated to 70 °C under strong stirring after $ZnAc_2 \cdot 2H_2O$ completely dissolved in ethanol. The mixture was injected into octyl ether−oleic acid solution (10 mL of octyl ether and 1.35 mL (4.5 mmol) of oleic acid) by a syringe at 80 °C, in which oleic acid acts as a surfactant. When the solution

* To whom correspondence should be addressed. E-mail: jiangjz@zju.edu.cn.
[†] ICNSM and Laboratory of New-Structured Materials, Depatment of Materials Science and Engineering, Zhejiang University.
[‡] INA.
[§] E-mail: jianglab@zju.edu.cn.
[||] Analysis and Testing Centre, Zhejiang University.

10.1021/jp0732763 CCC: $37.00
Published on Web 08/02/2007

temperature reached 130 °C, 0.13 mL of $Fe(CO)_5$ (1 mmol) was rapidly added into solution, and then the mixture was heated to 290 °C with a rate of 2 °C/min and refluxed at 290 °C for 2 h. During reaction the color of the solution varies from transparent to yellow and to black. After reaction, the solution was cooled to room temperature and excess ethanol was added into the flask. The products could be obtained by centrifugation of the solution at a rate of 10 000 rpm for 30 min. After discarding the supernatant, the precipitate was washed by methanol, ethanol, or chloroform. Final products obtained were dried in vacuum at 50 °C.

2.3. Characterization. Structural studies on the as-synthesized samples were carried out using transmission electron microscopy (TEM) and X-ray powder diffraction (XRD). TEM images and electron diffraction patterns were obtained on a JEOL 200CX microscope by dispersing powder samples in the dimethylbenzene and then dipping the liquid onto a carbon-coated copper grid. XRD measurements were performed using a Rigaku D/MAX-2550PC X-ray powder diffractometer with Bragg−Brentano geometry using Cu Kα irradiation in the 2θ range of 15−95°, a step of 0.02° and 4 s/step. The average grain size, d, and the root-mean square (rms) atomic-level strain, $\langle\epsilon^2\rangle^{1/2}$, within particles were estimated from the diffraction line broadening using the Williamson−Hall method.[25]

Magnetic studies, including zero-field cooling (ZFC), field cooling (FC), hysteresis, and relaxation measurements, were conducted on a physical property measure system (Quantum Design PPMS-9) and on a SQUID magnetometer MPMS-xl. Hysteresis curves were recorded at 10, 30, 100, and 300 K, and the zero-field cooling (ZFC) and field cooling (FC) curves were obtained under the applied field of 100 Oe for samples. Saturation magnetization (M_S), coercivity (H_C), and blocking temperature (T_B) were deduced from these measurements. Furthermore, magnetic relaxation spectra were recorded at different applied magnetic fields, 200, 500, 1000, 5000, 10 000, and 50 000 Oe at 5 K in order to study the stability of as-synthesized nanometer-sized $(Zn_{1-x}Fe_x)[Zn_xFe_{2-x}]O_4$ particles.

3. Results

3.1. Structural Studies. From the TEM images shown in Figure 1a, the as-synthesized nanocrystals are quite uniform in size. Grain size distribution was estimated by counting about 300 nanoparticles and characterized by a Gaussian function (solid line) in Figure 1d with an average grain size of 9.8 ± 0.2 nm and standard deviation of 30%. As shown in Figure 1c, these nanoparticles are crystalline, having a spinel structure. The high-resolution TEM image in Figure 1b shows the internal atomic lattice for a nanocrystal. The particle appears to be a single crystal and exhibits a 0.252 nm d-spacing for the (311) reflection. A typical XRD pattern of the as-synthesized $ZnFe_2O_4$ nanocrystals was shown in Figure 2. The $ZnFe_2O_4$ nanoparticles have a high degree of crystallinity. All of the peaks match well with Bragg reflections of the standard spinel structure (space group $Fd3m$). The average grain size is found to be about 10 nm, which is in good agreement with the result obtained by TEM in Figure 1, together with a small value $\langle\epsilon^2\rangle^{1/2} = 0.05\%$. The lattice parameter of an as-prepared sample is found to be 8.411(5) Å, slightly smaller than the 8.443 Å value reported for bulk zinc ferrite (PCPDF No. 89−4926). It is well-known that for zinc ferrite Zn ions at A sites and Fe ions at B sites are surrounded by four and six nearest oxygen anions, respectively. When the particle size decreases into nanometer-sized scale, surface area increases greatly, which enhances the energy of the system, making re-distribution of Zn and Fe ions possible. These nanometer-sized $(Zn_{1-x}Fe_x)[Zn_xFe_{2-x}]O_4$ particles could have a contraction in lattice, as observed in Figure 2. This is in agreement with the results obtained by other researchers.[26]

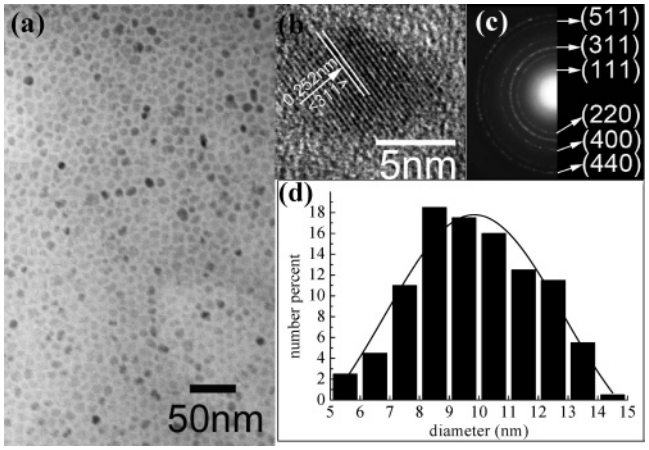

Figure 1. TEM and HRTEM measurements of $ZnFe_2O_4$ nanocrystals obtained by thermal decomposition. (a) Low-magnification TEM image of as-synthesized $ZnFe_2O_4$ nanoparticles. (b) High-resolution TEM image of a single $ZnFe_2O_4$ nanoparticle. The d-spacing is 0.252 nm corresponding to the (311) fringes of cubic $ZnFe_2O_4$. (c) SAED pattern of the $ZnFe_2O_4$ nanoparticle shown in a. The diffraction rings are attributed to the (111), (220), (311), (400), (511), and (440) planes, respectively. (d) Size distribution of $ZnFe_2O_4$ nanocrystals obtained from counting 300 nanoparticles.

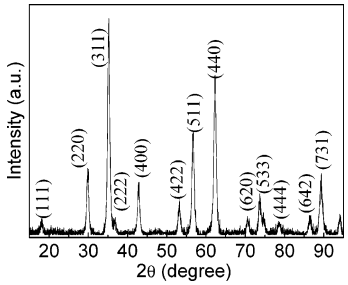

Figure 2. XRD pattern of as-synthesized $ZnFe_2O_4$ nanoparticles.

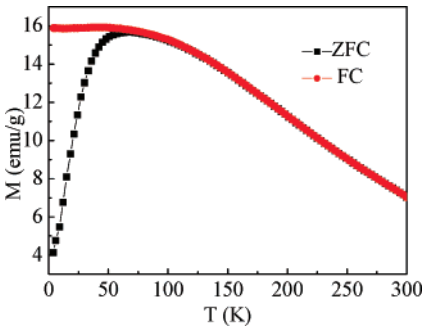

Figure 3. Zero-field cooling and field-cooling magnetization data measured in an applied field of 100 Oe for as-synthesized $ZnFe_2O_4$ nanoparticles.

3.2. Magnetic Studies. Detailed magnetic measurements, i.e., zero-field cooling and field cooling magnetization vs temperature, magnetic hysteresis loops at several temperatures, relaxation under different applied fields at 5 K, have been carried out in order to study the magnetic properties of the as-synthesized $(Zn_{1-x}Fe_x)[Zn_xFe_{2-x}]O_4$ nanoparticles. Figure 3 shows the temperature dependence of magnetization by the ZFC and FC procedures from 5 to 300 K in an applied magnetic field of 100 Oe. The curve shows a cusp at $T_B = 65 \pm 2$ K as expected for superparamagnetic nanoparticles, below which the

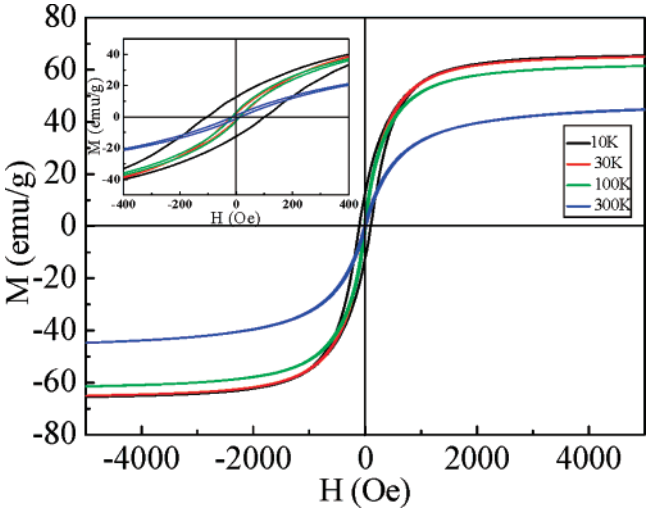

Figure 4. Magnetization vs applied magnetic field for as-synthesized $ZnFe_2O_4$ nanoparticles at different temperatures. Inset shows these curves with a field range from −400 to +400 Oe.

TABLE 1: Size and Magnetic Parameters for As-Synthesized $ZnFe_2O_4$ Nanoparticles at 10 K

$\langle d\rangle_{TEM}$ (nm)	9.8	M_0 (emu·g^{-1})	62.5
M_S (emu·g^{-1})	65.4	χ (emu·g^{-1}·Oe^{-1})	6.6×10^{-4}
H_C (Oe)	102.4	μ_{eff} (μ_B)	1.7×10^4

system is blocked. Also magnetic irreversibility between ZFC and FC curves can be noticed from T_B up to $T_{irr} \approx 90$ K, where both curves merge with each other. This difference between T_B and T_{irr} values reflects the contribution of the larger particles ($\langle d\rangle$ from 9 to 15 nm, as observed in TEM images) to the magnetization as they unblock at higher temperatures.

The blocking temperature signals the range for which the time scale of magnetization measurements equals the relaxation time, and thus the anisotropy constant can be estimated from the T_B value of the ZFC curve:[27]

$$K_{eff}V = k_B T_B \ln(\tau/\tau_0) \quad (1)$$

where K_{eff} is the effective anisotropy constant, V is the particle volume, k_B is the Boltzmann's constant, τ is the superparamagnetic relaxation time, and τ_0 is a factor of the order of 10^{-9}−10^{-12}.[28−30] From eq 1 and with use of the T_B value from ZFC data, a value of $K_{eff} = 46$ kJ/m^3 was obtained for the as-synthesized $(Zn_{1-x}Fe_x)[Zn_xFe_{2-x}]O_4$ nanoparticles. This value compares well to the values previously reported for other iron oxide cubic spinels; e.g., $(Fe^{+2})[Fe^{3+}]_2O_4$ has $K_{eff} = 20$−35 kJ·m^{-3}.[31]

Figure 4 shows magnetic hysteresis loops for as-synthesized $(Zn_{1-x}Fe_x)[Zn_xFe_{2-x}]O_4$ nanoparticles at different temperatures $T = 10$, 30, 100, and 300 K. Table 1 lists values of saturation magnetization and coercivity at 10 K for the as-synthesized $(Zn_{1-x}Fe_x)[Zn_xFe_{2-x}]O_4$ nanoparticles. We found that the value of saturation magnetization is about 65.4 emu·g^{-1} at $T =$ 10 K. It is known that the inversion degree in $ZnFe_2O_4$ results in large magnetization values originated in the uncompensation of the antiferromagnetic B sublattice, which is known to be fully populated in normal configuration. In Table 2 we listed previously reported values of M_S for zinc ferrite nanoparticles prepared by various methods. The broad range of $M_S \sim 12$−88 emu·g^{-1} in Table 2 reflects the fact that M_S strongly depends on the synthesis method used. Our present values of M_S lay within these values, indicating that the redistribution of Fe ions between A and B sites occurs in the as-synthesized $(Zn_{1-x}Fe_x)[Zn_xFe_{2-x}]O_4$ nanoparticles.[32] Magnetization data taken at $T = 10$ K show that the $M(H)$ cycle remains open up to about 1.3 kOe, reflecting magnetic irreversibility below this field value. This result is much lower than previous reports on highly defective $ZnFe_2O_4$ and $CuFe_2O_4$ nanoparticles prepared by high-energy ball milling,[38,45] where high-field irreversibility is observed up to 60−90 kOe. This high field magnetization irreversibility implies an anisotropy field larger than the magnetocrystalline or shape anisotropies usually observed for small particles and has been assigned to defect-enhanced magnetic anisotropy.[46−48] Further analyses of the $M(H)$ data showed that the magnetization does not saturate even for our highest fields ($H = 50$ kOe), indicating a magnetically hard component that can be associated to surface spin disorder. The magnetization showed a nearly linear dependence on H for fields $H > 3$ kOe, and thus the data were fitted in this region using the expression

$$M = M_0 + \chi H \quad (2)$$

where M_0 is the extrapolated magnetization at zero field and χ is the high field susceptibility. The resulting values were $M_0 =$ 62.5 emu·g^{-1} and $\chi = (6.6 \pm 0.6) \times 10^{-4}$ emu·g^{-1}·Oe^{-1}. The

TABLE 2: Reported Values of Saturation Magnetization for $ZnFe_2O_4$ Nanoparticles Prepared by Various Methods

M_S (emu·g^{-1})	temp (K)	size (nm)	synthesis method	ref no.
65.4	10	9.8	thermal decomposition	this work
38	60	4	hydrothermal method	32
25	5	12	Ultrasound-assisted emulsion	33
78	5	6.6	polyol method	34
53.9	5	14.8	polyol method	34
70	3	3.7	oil-in-water micelles	35
61.87	80	300	hydrothermal in ammonia solution	36
11.9	2	32	self-propagating combustion	37
∼37	4.2	47	ball milling	38
22	5	8.1	supercritical sol−gel + drying at 513 K	39
73	10	10.3	supercritical sol−gel + drying at 513 K + ball milling for 10 h	39
38	4.2	5−20	hydrothermal in supercritical methanol	40
20.7	4.2	36	ball milling	41
40.3	4.2	50	ball milling + calcinations at 773 K	41
10	300	11	ball milling	42
75	300	14	ball milling	42
58	5	9	ball milling	43
88.4	4.2	10	ball milling	8
46.9	4.2	55	co-precipitation at 373 K	44
26.4	5	29	co-precipitation at 373 K + calcination	44
56.6	300	thin film	pulsed lased deposition	15

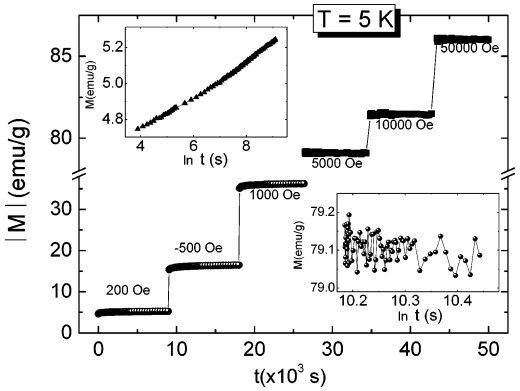

Figure 5. Relaxation patterns at 5 K under the fields indicated. Upper left inset: relaxation pattern under $H = 200$ Oe showing logarithmic time dependence of $M(t)$. Lower right inset: relaxation pattern under 50 kOe, where no time evolution is detected.

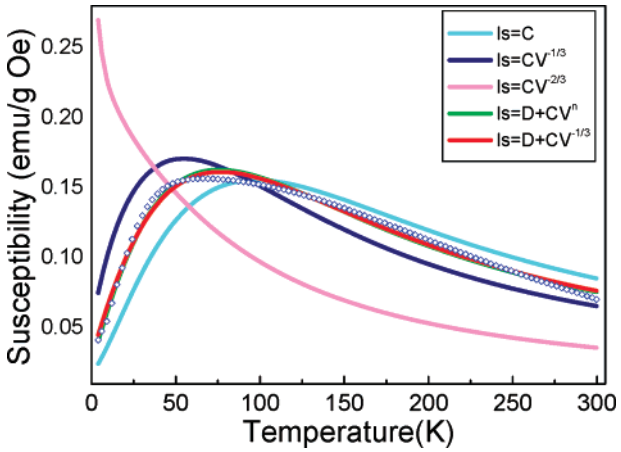

Figure 6. ZFC data together with fitting results using different models. Details are given in the text.

effective magnetic moment *per particle* extracted from the M_0 value and with use of the average particle size from TEM measurements was $\mu_{eff} = 1.7 \times 10^4\ \mu_B$. In Figure 5 we show the relaxation data of the magnetization under different applied fields 0.2, −0.5, −1, 5, −10, and 50 kOe at the same temperature of 5 K (i.e., well below the blocking temperature). For each field, the relaxation was measured for about 8000 s, changing the field from positive to negative for each successive measurement, to allow the sample to relax to a different state crossing the $M = 0$ magnetization. The curves obtained for $H < 1000$ Oe show clear relaxation effects (see the upper inset of Figure 5) with a logarithmic time dependence, indicating that domain rotation is not complete. For $H \geq 5000$ Oe the system shows negligible relaxation effects within experimental error, indicating that there is no magnetic viscosity.[33]

4. Discussion

In a few-nanometer particle the surface/volume ratio can be increased notably, so that a major fraction (up to 50−70%) of the particle atoms can be on the surface. For our $ZnFe_2O_4$ nanoparticles having ca. 10 nm, the large fraction of the total spins at the surface will have a non-collinear configuration with respect to the core ones, due to broken exchange bonds and symmetry. This results in an increase in the net magnetic moment of the single-domain $ZnFe_2O_4$ particle. The redistribution of Zn and Fe ions at both A and B sites in $ZnFe_2O_4$ particles also change the net magnetization of particles. It is well-known that three kinds of interactions, A−A, B−B, and A−B superexchange interactions, exist in spinel ferrites, in which A−B interaction is much larger than the others. In bulk $ZnFe_2O_4$ having normal cationic configuration, the absence of magnetic ions at A sites (populated by nonmagnetic Zn) results in weak antiferromagnetic exchange interactions within Fe atoms at B sites, making bulk $ZnFe_2O_4$ antiferromagnetic below 10 K. In the as-synthesized $(Zn_{1-x}Fe_x)[Zn_xFe_{2-x}]O_4$ nanoparticles, a fraction of Fe and Zn ions occupy A and B sites, respectively. The Fe−Fe interaction between A−B sublattices, which is ferromagnetic, is much stronger than Fe−Fe ions at B−B sites. This largely enhances saturation magnetization and magnetic transition temperature above 300 K, as observed in Figure 4.

To further study the magnetic structure of the as-synthesized $(Zn_{1-x}Fe_x)[Zn_xFe_{2-x}]O_4$ particles, the ZFC data were analyzed by various models taking into account of particle size distribution, surface effect, and ferromagnetic or antiferromagnetic particles. The magnetic susceptibility for a single particle with volume V is given by Wohlfarth[49] as

$$\chi = M_S^2 V/3k_BT \qquad \text{when } T \geq T_B \tag{3}$$

$$\chi = M_S^2 V/3K \qquad \text{when } T < T_B \tag{4}$$

where M_S is the magnetization of the particle, which was assumed to be temperature-independent in the fitting process. For ferromagnetic particles, marked as model 1, M_S does not depend on the particle volume. However, for antiferromagntic particles, M_S depends on the particle volume. In the fitting process, we used the dependence of the net moment on V proposed by Richardson[50] for antiferromagnetic particles, marked as model 2; i.e.,

$$M_S = CV^{-2/3} \tag{5}$$

where C depends on the atomic moment for the material. For the surface spin canting effect, we assume that the saturation magnetization is proportional to the percentage of surface magnetic ions, marked as model 3, i.e.,

$$M_S = CV^{-1/3} \tag{6}$$

where C is a fitting parameter. On the basis of the consideration mentioned above, a combination of ferromagnetic contribution with surface spin canting was suggested, in which the relationships between M_S and V, marked as model 4 and model 5, are expressed as

$$M_S = D + CV^{-1/3} \tag{7}$$

$$M_S = D + CV^n \tag{8}$$

where C is a fitting parameter. Fitting results using eqs 3−8 are shown in Figure 6 by using the particle size distribution of the as-synthesized $(Zn_{1-x}Fe_x)[Zn_xFe_{2-x}]O_4$ particles: $f(d) = A/(\sqrt{2\pi}\sigma)\ \exp[-((d - d_0)^2/2\sigma^2)]$ with $\sigma = 3 \pm 1$ nm and $d_0 = 9.8 \pm 0.2$ nm, which was obtained from TEM in Figure 1. We found that (1) pure antiferromagnetic nanoparticles cannot fit ZFC data at all, indicating our $(Zn_{1-x}Fe_x)[Zn_xFe_{2-x}]O_4$ particles are not antiferromagnetic, and (2) using model 1 and model 3, fitting gets better. However, these two fitting curves are located at the two sides of the measured ZFC data, which indicate that the real magnetic structure of our as-prepared $(Zn_{1-x}Fe_x)[Zn_xFe_{2-x}]O_4$ particles might be a combination of the models. Indeed, the fitting to the ZFC data becomes much better using model 4 or model 5, as shown in Figure 6. We found the n value in model

5 of −0.30, which is very close to $-1/3$ for model 4. Thus, we conclude that our as-synthesized $(Zn_{1-x}Fe_x)[Zn_xFe_{2-x}]O_4$ particles have both a ferromagnetic component, which could be resulted from by the re-distribution of Fe around A and B sites, and a surface spin canting component from large fraction of surface ions for nanometer-sized particles. We believe that the resulting magnetic moment arising from these two mechanisms results in the different behavior observed in our as-synthesized $(Zn_{1-x}Fe_x)[Zn_xFe_{2-x}]O_4$ nanoparticles, as compared to bulk $ZnFe_2O_4$. More specific measurements (e.g., in-field Mossbauer data) are needed for a trustable estimation of the relative contributions from surface and bulk in these nanoparticles.

5. Conclusions

In summary, we have synthesized zinc ferrite nanocrystals using thermal decomposition, which showed relatively narrow particle size distribution with an average particle size $\langle d \rangle = 9.8 \pm 0.2$ nm and standard deviation of 30%. From our magnetization data we inferred a ferromagnetic structure of the particles with a saturation magnetization of 44.9 emu·g^{-1} at room temperature. This value increases to $M_S = 65.4$ emu·g^{-1} for $T = 10$ K, among the largest found in partially inverted $ZnFe_2O_4$ spinel. Below $T_B = 68 \pm 2$ K the system is blocked by interparticle interactions. The as-synthesized zinc ferrite nanocrystals are magnetically stable. By fitting ZFC data using various models, we conclude that the magnetic behavior of the as-synthesized zinc ferrite nanocrystals can be related to two different mechanisms: ferromagnetic coupling of Fe ions at A−B sites in the $(Zn_{1-x}Fe_x)[Zn_xFe_{2-x}]O_4$ particles and surface spin canting. The change observed in the magnetic properties of particles with different particle sizes in the present work suggests that this could be a useful way to design novel magnetic materials.

Acknowledgment. Financial support from the National Natural Science Foundation of China (Grant Nos. 50341032, 50425102, and 50601021), Zhejiang University-Helmholtz cooperation fund, the Ministry of Education of China (Grant Nos. 2.005E+10 and 2005-55), and Zhejiang University is gratefully acknowledged. G.F.G. acknowledges financial support from Ministry of Education (MEC) and University of Zaragoza through the Ramon y Cajal Program.

References and Notes

(1) Alves, C. R.; Aquino, R.; Depeyrot, J.; P Cotta, T. A.; Sousa, M. H.; Tourinho, F. A.; Rechenberg, H. R.; Goya, G. F. *J. Appl. Phys.* **2006**, *99*, 08M905.
(2) Daliya, S. M.; Juang, R. S. *Chem. Eng. J.*, in press.
(3) Tung, L. D.; Kolesnichenko, V.; Caruntu, G.; Caruntu, D. *Physica B* **2002**, *319*, 116.
(4) Chu, X.; Liu, X.; Meng, G. *Sens. Actuators, B* **1999**, *55*, 19.
(5) Sohn, B. H.; Cohen, R. E. *Chem. Mater.* **1997**, *9*, 264.
(6) Jiang, J. Z.; Wynn, P. *Nanostuct. Mater.* **1999**, *12*, 737.
(7) Sepelak, V.; Wilde, L.; Steinike, U.; Becker, K. D. *Mater. Sci. Eng., A* **2004**, *375*−*377*, 865.
(8) Goya, G. F.; Rechenberg, H. R. *J. Magn. Magn. Mater.* **1999**, *196*, 191.
(9) Ozcan, S.; Kaynar, B.; Can, M. M.; Firat, T. *Mater. Sci. Eng., B* **2005**, *121*, 278.
(10) Atif, M.; Hasanain, S. K.; Nadeem, M. *Solid State Commun.* **2006**, *138*, 416.
(11) Plocek, J.; Hutlova, A.; Niznansky, D.; Bursık, J.; Rehspringer, J. L.; Micka, Z. *J. Non-Cryst. Solids* **2003**, *315*, 70.
(12) Shenoy, S. D.; Joy, P. A.; Anantharaman, M. R. *J. Magn. Magn. Mater.* **2003**, *269*, 217.
(13) Martın, J. L.; Vidales, D.; Lopez, D. A.; Vila, E.; Lopez, F. A. *J. Alloys Compd.* **1999**, *287*, 276.
(14) Komar, P. In *Handbook of Microemulsion Science and Technology*; Mittal, K. L., Ed.; Dekker: New York, 1999.
(15) Wakiya, N.; Muraoka, K.; Kiguchi, T.; Mizutani, N.; Shinozaki, K. *J. Magn. Magn. Mater.* **2007**, *310*, 2546.
(16) Roy, M. K.; Verma, H. C. *J. Magn. Magn. Mater.* **2006**, *306*, 98.
(17) Li, F. S.; Wang, H. B.; Wang, L.; Wang, J. B. *J. Magn. Magn. Mater.* **2006**, *309*, 295.
(18) Li, Y.; Zhao, J. P.; He, X. D. *Mater. Sci. Eng., B* **2004**, *106*, 196.
(19) Sivakumar, M.; Towata, A.; Yasui, K.; Tuziuti, T.; Iida, Y. *Curr. Appl. Phys.* **2006**, *6*, 591.
(20) Kang, E.; Park, J.; Hwang, Y.; Kang, M.; Park, J. G.; Hyeon, T. *J. Phys. Chem. B* **2004**, *108*, 13932.
(21) Zeng, H.; Philp, M. R.; Wang, S. X.; Sun, S. X. *J. Am. Chem. Soc.* **2004**, *126*, 11485.
(22) Easom, K. A.; Klabunde, K. J. *Polyhedron* **1994**, *13*, 1197.
(23) Rockenberger, J.; Scher, E. C.; Alivisatos, A. P. *J. Am. Chem. Soc.* **1999**, *121*, 11595.
(24) Guo, Q.; Teng, X.; Rahman, S.; Yang, H. *J. Am. Chem. Soc.* **2003**, *125*, 630.
(25) Williamson, G. K.; Hall, W. H. *Acta Metall.* **1953**, *1*, 22.
(26) Wang, L.; Zhou, Q. G.; Li, F. S. *Phys. Status Solidi B* **2004**, *241*, 377.
(27) Duarte, E. L.; Itri, R.; Lima, E., Jr.; Baptista, M. S.; Berquó, T. S.; Goya, G. F. *Nanotechnology* **2006**, *17*, 5549.
(28) Johansson, C.; Hanson, M.; Hendriksen, P. V. *J. Magn. Magn. Mater.* **1993**, *122*, 125.
(29) Linderoth, S.; Balcells, L.; Laberta, A. *J. Magn. Magn. Mater.* **1993**, *124*, 269.
(30) Dickson, D. P. E.; Reid, N. M. K.; Hunt, C. *J. Magn. Magn. Mater.* **1993**, *125*, 345.
(31) Lima, E., Jr.; Brandl, A. L.; Arelaro, A. D.; Goya, G. F. *J. Appl. Phys.* **2006**, *99*, 083908.
(32) Upadhyay, C.; Verma, H. C.; Sathe, V.; Pimpale, A. V. *J. Magn. Magn. Mater.* **2007**, *312*, 271.
(33) Sivakumar, M.; Takami, T.; Iida, Y. *J. Phys. Chem. B* **2006**, *110*, 15234.
(34) Ammar, A.; Jouini, N.; Fievet, F.; Beji, Z.; Smiri, L.; Moline, P.; Danot, M.; Greneche, J. M. *J. Phys.: Condens. Matter* **2006**, *18*, 9055.
(35) Hochepied, J. F.; Bonville, P.; Pileni, M. P. *J. Phys. Chem. B* **2000**, *104*, 905.
(36) Yu, S. H.; Fujino, T.; Yoshimura, M. *J. Magn. Magn. Mater.* **2003**, *256*, 420.
(37) Xue, H.; Li, Z. H.; Wang, X. X.; Fu, X. Z. *Mater. Lett.* **2007**, *61*, 347.
(38) Goya, G. F.; Rechenberg, H. R. *J. Magn. Magn. Mater.* **1999**, *203*, 141.
(39) Hamdeh, H. H.; Ho, J. C.; Oliver, S. A.; Willey, R. J.; Oliveri, G.; Busca, G. *J. Appl. Phys.* **1997**, *81*, 1851.
(40) Bluncson, C. R.; Thompson, G. K.; Evans, B. J. *Hyperfine Interact.* **1994**, *90*, 353.
(41) Goya, G. F.; Rechenberg, H. R.; Chen, M.; Yelon, W. B. *J. Appl. Phys.* **2000**, *87*, 8005.
(42) Chinnasamy, C. N.; Narayanasamy, A.; Ponpandian, N.; Chattopadhyay, K.; Guérault, H.; Greneche, J. M. *J. Phys.: Condens. Matter* **2000**, *12*, 7795.
(43) Burghart, F. J.; Potzel, W.; Kalvius, G. M.; Schreier, E.; Grosse, G.; Noakes, D.; Martin, A.; Krausse, M. K. *Physica B* **2000**, *289*−*290*, 286.
(44) Kamiyama, T.; Haneda, K.; Sato, T.; Ikeda, S.; Asano, H. *Solid State Commun.* **1992**, *81*, 563.
(45) Jiang, J. Z.; Goya, G. F.; Rechenberg, H. R. *J. Phys.: Condens. Matter* **1999**, *11*, 4063.
(46) Kodama, R, H.; Berkowitz, A. E.; McNiff, E. J.; Foner, S. *Phys. Rev. Lett.* **1996**, *77*, 394.
(47) Parker, F. T.; Spada, F. E.; Cox, T. J.; Berkowitz, A. E. *J. Appl. Phys.* **1995**, *77*, 5833.
(48) Lin, D.; Nunez, A. C.; Majkrzak, C. F.; Berkowitz, A. E. *J. Magn. Magn. Mater.* **1995**, *145*, 343.
(49) Wohlfarth, E. P. *Phys. Lett. A* **1979**, *70*, 489.
(50) Richardson, J. T.; Yiagas, D. I.; Turk, B. *J. Appl. Phys.* **1991**, *70*, 6977.